Pressure-Tunable Large Anomalous Hall Effect in Ferromagnetic Metal $LiMn_6Sn_6$

Lingling Gao(高玲玲)[1†], Junwen Lai(赖俊文)[2†], Dong Chen(陈栋)[3,4†], Cuiying Pei(裴翠颖)[1], Qi Wang(王琦)[1,5], Yi Zhao(赵毅)[1], Changhua Li(李昌华)[1], Weizheng Cao(曹渭征)[1], Juefei Wu(吴珏霏)[1], Yulin Chen(陈宇林)[1,5,6], Xingqiu Chen(陈星秋)[2,7], Yan Sun(孙岩)[2,7*], Claudia Felser[3*], and Yanpeng Qi(齐彦鹏)[1,5,8*]

[1]*School of Physical Science and Technology, ShanghaiTech University, Shanghai 201210, China*
[2]*Shenyang National Laboratory for Materials Science, Institute of Metal Research, Chinese Academy of Sciences, Shenyang 110016, China*
[3]*Max Planck Institute for Chemical Physics of Solids, Dresden 01187, Germany*
[4]*College of Physics, Qingdao University, Qingdao 266071, China*
[5]*ShanghaiTech Laboratory for Topological Physics, ShanghaiTech University, Shanghai 201210, China*
[6]*Department of Physics, Clarendon Laboratory, University of Oxford, Parks Road, Oxford OX1 3PU, UK*
[7]*School of Materials Science and Engineering, University of Science and Technology of China, Shenyang 110016, China*
[8]*Shanghai Key Laboratory of High-resolution Electron Microscopy, ShanghaiTech University, Shanghai 201210, China*

(Received 17 January 2024; accepted manuscript online 17 April 2024)

Recently, giant intrinsic anomalous Hall effect (AHE) has been observed in the materials with kagome lattice. Here, we systematically investigate the influence of high pressure on the AHE in the ferromagnet $LiMn_6Sn_6$ with clean Mn kagome lattice. Our *in situ* high-pressure Raman spectroscopy indicates that the crystal structure of $LiMn_6Sn_6$ maintains a hexagonal phase under high pressures up to 8.51 GPa. The anomalous Hall conductivity (AHC) σ_{xy}^{A} remains around $150\,\Omega^{-1}\cdot\mathrm{cm}^{-1}$, dominated by the intrinsic mechanism. Combined with theoretical calculations, our results indicate that the stable AHE under pressure in $LiMn_6Sn_6$ originates from the robust electronic and magnetic structure.

DOI: 10.1088/0256-307X/41/5/057302

Anomalous Hall effect (AHE),[1,2] arising from the "anomalous" transverse group velocity of carriers, has been experimentally observed in materials with broken time-reversal symmetry, typically in a ferromagnetic phase. Although it was experimentally discovered more than a century ago, the microscopic mechanism of AHE remains an unsolved topic in condensed matter physics.[3,4] It has been generally accepted that spin–orbit coupling and spin splitting are two essential ingredients for the AHE. In general, AHE can be broadly engendered by two classes of mechanisms:[3] the extrinsic disorder-induced effects (e.g., skew scattering and side jump),[5–7] or the intrinsic Berry-curvature effect.[8] Nevertheless, as the AHE continues to be discovered in various material systems, it not only deepens our understanding of such a striking electronic transport phenomenon,[9] but also paves the way for applications of next-generation spintronic devices.[10]

Recently, giant intrinsic AHE induced by the large Berry curvature has been observed in the materials with kagome lattice,[11] such as the bilayer Fe kagome ferromagnet Fe_3Sn_2,[12,13] noncollinear antiferromagnet Mn_3Sn,[14] and magnetic Weyl semimetal $Co_3Sn_2S_2$.[15–17] In the kagome family, RMn_6Sn_6 (R = trivalent rare earth elements) has been a special one and attracted growing interest due to the pristine Mn kagome lattice.[18–23] We have successfully synthesized high-quality RMn_6Sn_6 (R = Tb, Dy, Ho) single crystals and observed large anomalous Hall conductivity (AHC) arising from the intrinsic mechanism.[24] More interestingly, the R elements in the RMn_6Sn_6 family can be completely replaced by Li, Mg, or Ca,[19,25,26] which not only reduce the number of valence electrons but also change the magnetic states. Thus, the RMn_6Sn_6 family with clean Mn kagome lattice supply an excellent platform to tune electronic and magnetic states and explore larger AHE.

Pressure is a clean and useful means to tune the interatomic distance, and to engineer the electronic and, subsequently, the macroscopic physical properties of the system.[27–30] To our knowledge, only a few experimental observations of high pressure modulated AHE have been reported up to date.[31–36] In this Letter, we focus on $LiMn_6Sn_6$, one member in the RMn_6Sn_6 family with clean Mn kagome lattice, and study the pressure effect on the AHE employing *in situ* high-pressure Raman spectroscopy, Hall transport measurements and first-principles calculations. We find that the AHE is quite stable against external pressure within our measurement range, which has been shown to originate from the robust electronic and magnetic structure using density-functional theory (DFT). Our results demonstrate that $LiMn_6Sn_6$ with clean Mn

†These authors contributed equally to this work.
*Corresponding authors. Email: qiyp@shanghaitech.edu.cn; claudia.felser@cpfs.mpg.de; sunyan@imr.ac.cn
© 2024 Chinese Physical Society and IOP Publishing Ltd

kagome lattice displays excellent AHE upon compression and potential applications to the next-generation spintronic devices.

The single crystals of $LiMn_6Sn_6$ were grown by the self-flux method and the details of crystal growth are illustrated in Ref. [19]. The single crystal diffraction patterns were obtained using a Bruker dual sources single crystal x-ray diffractometer at room temperature, and the x-ray source comes from a molybdenum target. An *in situ* high-pressure Raman spectroscopy investigation was performed using a Raman spectrometer (Renishaw inVia, UK) with a laser excitation wavelength of 532 nm and low-wavenumber filter. A symmetric diamond anvil cell (DAC) with anvil culet sizes of 400 μm was used, with silicon oil as the pressure transmitting medium. The high-pressure electrical transport measurements were performed on Quantum Design PPMS-9T. *In situ* high-pressure transport measurements were conducted on a nonmagnetic DAC with 600 μm-culet diamond. The schematic plot of the DAC electrical transport measurement device can be found in Refs. [36,37]. A cubic BN/epoxy mixture layer was inserted between BeCu gaskets and Pt electrical leads as an insulator layer. A freshly cleaved single-crystal piece of $\sim 200\,\mu m \times 150\,\mu m \times 25\,\mu m$ was loaded with NaCl powder as the pressure transmitting medium. A five-probe method was used to measure the longitudinal and Hall electrical resistivity. The longitudinal current applied within the ab plane (in-plane), and the magnetic field is along the c axis (out-of-plane). The pressure was determined by the ruby luminescence method.[38] In order to remove the longitudinal resistivity contribution due to voltage probe misalignment, we extracted the pure Hall resistivity by the equation $\rho_{yx} = [\rho(+\mu_0 H) - \rho(-\mu_0 H)]/2$. Correspondingly, the longitudinal resistivity component is obtained using $\rho_{xx}(\mu_0 H) = [\rho(+\mu_0 H) + \rho(-\mu_0 H)]/2$.

To calculate the electronic band structure, we took the experimentally measured lattice constants as the starting point and relaxed the atomic positions. The pressure conditions were simulated by shrinking the volume of primitive cells with the relaxation of lattice constants and atomic positions. The electronic and magnetic structure calculations were performed by using the code of Vienna *ab initio* Simulation Package (VASP)[39] based on density functional theory with projected augmented wave potential. The exchanged and correlation energies were considered in the generalized gradient approximation (GGA), following the Perdew–Burke–Ernzerhof parametrization scheme.[40] The cut-off energy of plane wave basis was set to be 500 eV. To calculate the intrinsic anomalous Hall effect, we projected the Bloch wave functions into maximally localized Wannier functions (MLWFs).[41] The tight binding model Hamiltonians were constructed based on the overlap of MLWFs. Based on tight binding model Hamiltonians, the intrinsic AHCs were calculated by the Kubo formula in linear response approximation:[42]

$$\sigma_{yx}(E_{\rm F}) = e^2\hbar\left(\frac{1}{2\pi}\right)^3 \int_{\boldsymbol{k}} d\boldsymbol{k} \sum\nolimits_{E(n,\boldsymbol{k})<E_{\rm F}} f(n,\boldsymbol{k})\Omega_{n,yx}(\boldsymbol{k}), \tag{1}$$

$$\begin{aligned}\Omega^{z}_{n,yx}(\boldsymbol{k}) &= {\rm Im}\sum_{n'\neq n}\Big\{\big[\langle u(n,\boldsymbol{k})\,|\,\hat{v}_y\,|\,u(n',\boldsymbol{k})\rangle\langle u(n',\boldsymbol{k})\,|\,\hat{v}_x\,|\,u(n,\boldsymbol{k})\rangle \\ &\quad - (x\leftrightarrow y)\big]\big[E(n,\boldsymbol{k}) - E(n',\boldsymbol{k})\big]^{-2}\Big\},\end{aligned} \tag{2}$$

where $\hat{v}_{x(y)} = \frac{1}{\hbar}\frac{\partial H(\boldsymbol{k})}{\partial k_{x(y)}}$ is the velocity operator, $E\,(n,\,\boldsymbol{k})$ is the eigenvalue for the n-th eigen states of $|u\,(n,\,\boldsymbol{k})\rangle$, and $f\,(n,\,\boldsymbol{k})$ is the Fermi–Dirac distribution. A dense k-grid of $250 \times 250 \times 250$ was used in the integral.

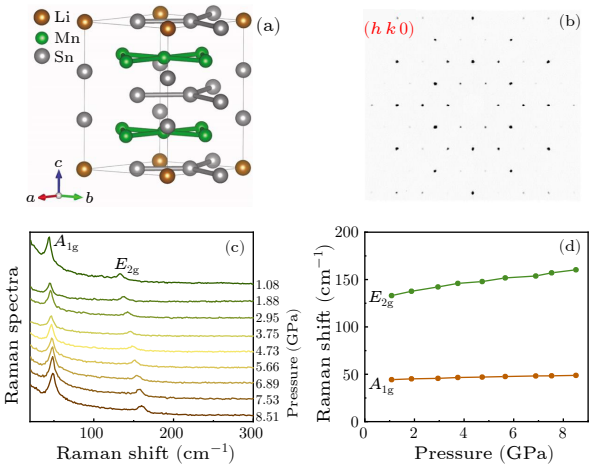

Fig. 1. (a) Crystal structure of $LiMn_6Sn_6$. The brown, green, and silver balls represent Li, Mn, and Sn, respectively. (b) Single crystal diffraction patterns in the reciprocal space along the (h k 0) direction. (c) Raman spectra at various pressures for $LiMn_6Sn_6$ at room temperature. (d) Raman shift for $LiMn_6Sn_6$ in compression. The vibration modes display in increasing wavenumber order.

As shown in Fig. 1(a), $LiMn_6Sn_6$ has the same crystal structure with the RMn_6Sn_6 compounds.[24–26] The single crystal diffraction pattern along the (h k 0) direction is displayed in Fig. 1(b), showing hexagonal symmetry. At ambient pressure, $LiMn_6Sn_6$ exhibits a ferromagnetic (FM) transition at $T_{\rm c} = 380$ K, and the easy plane is parallel to the ab plane (see Fig. S1 in the Supplementary Material).[19] The structure stability of $LiMn_6Sn_6$ is confirmed by *in situ* Raman spectroscopy measurements. Figure 1(c) shows the Raman spectra of $LiMn_6Sn_6$ under pressure up to 8.51 GPa. The assignments of the modes of $LiMn_6Sn_6$ at 1.08 GPa are given as $A_{1g} = 44.3\,{\rm cm}^{-1}$ and $E_{2g} = 132.84\,{\rm cm}^{-1}$. The profile of the spectra remains similar below 8.51 GPa, whereas the observed modes exhibit blue shift [Fig. 1(d)], thus showing the normal pressure behavior.[43] Our Raman results indicate that the structure of $LiMn_6Sn_6$ is robust and does not experience structural phase transition up to 8.51 GPa.

We performed two independent runs of transport experiments (run 1 and run 2). Figure 2(a) displays the longitudinal resistivity $\rho_{xx}(T)$ as a function of temperature from 1.8 K to 300 K in run 1. All of the resistivity curves exhibit metallic behavior at selected pressures, which are consistent with the resistivity curve at ambient pressure. The data of magnetoresistance (MR = $[\rho_{xx}(\mu_0 H) - \rho_{xx}(0)]/\rho_{xx}(0) \times 100\%$) have been normalized in Figs. 2(b)–2(f)) and Fig. S2 for runs 1 and 2, respec-

tively. The MR curves also show similar characteristics to that under ambient pressure, and visibly change at 50 K for different pressures. When T is below 50 K, the value of MR is positive, reveals the dominant role of Lorenz force in controlling MR process. At high temperature, it becomes negative owing to the suppressed spin scattering by magnetic field. The magnitude of the MR gradual decreases at high pressure up to 7.11 GPa.

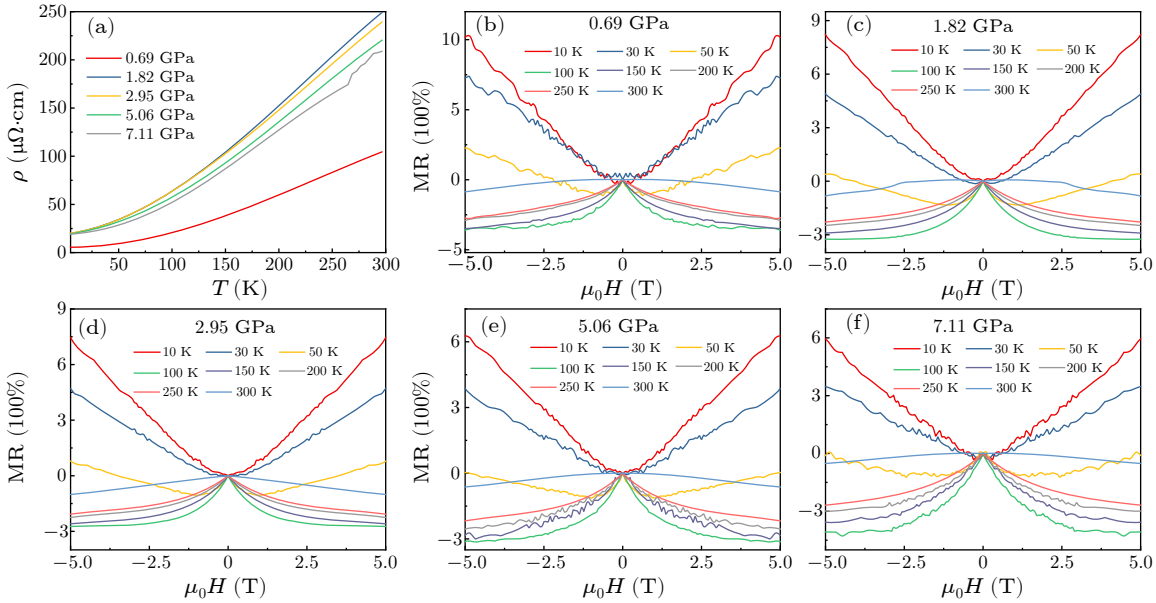

Fig. 2. (a) Temperature dependence of electric resistivity $\rho_{xx}(T)$ under high pressures. (b)–(f) Field dependence of magnetoresistance (MR) at various temperatures and selected pressures in run 1.

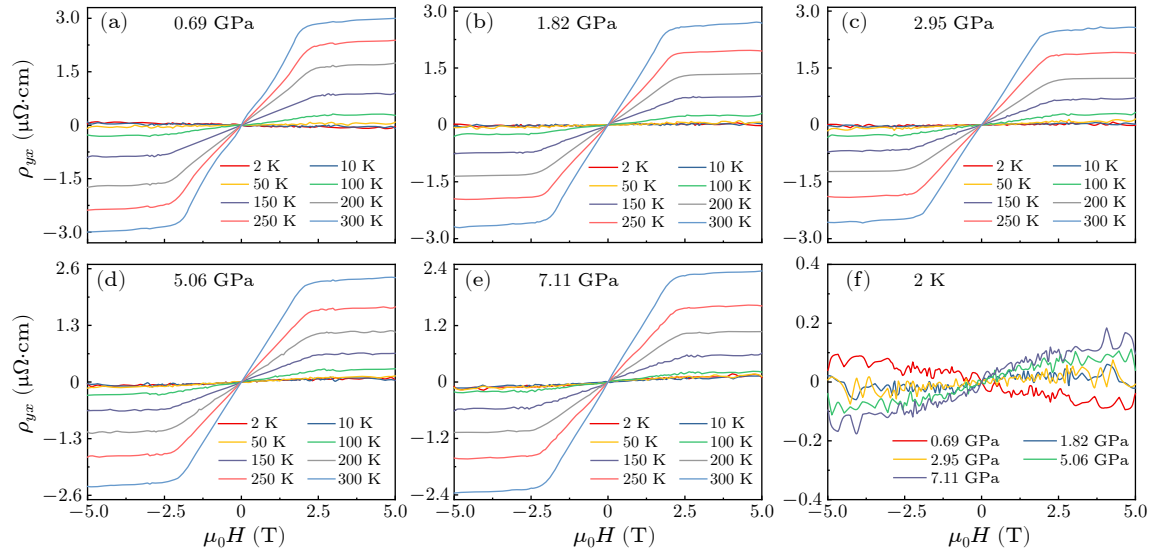

Fig. 3. (a)–(f) Field dependence of Hall resistivity ρ_{yx} at various temperature and selected pressures in run 1.

We performed the Hall effect measurements to evaluate the pressure effect on the AHE of $LiMn_6Sn_6$. Figure 3 and Fig. S3 in the Supplementary Material show the field dependence of the Hall resistivity $\rho_{yx}(\mu_0 H)$ at selected pressures in runs 1 and 2, respectively. As can be seen, the $\rho_{yx}(\mu_0 H)$ data at each pressure share similar features as those at ambient pressure.[19] At high temperature, the ρ_{yx} increases dramatically as the magnetic field increases and saturates at ~ 2 T, exhibiting typical features of AHE. Moreover, the saturated magnetic field H_s of Hall resistivity is insensitive to pressure and remains almost unchanged up to 7.11 GPa, which illustrates that the magnetization behavior of $LiMn_6Sn_6$ is stable against pressure. However, at low temperature, the anomalous Hall resistivity becomes too weak to be observed due to the reduction of resistivity, and the ordinary Hall resistivity is dominant. The slope of Hall resistivity is negative for 0.69 GPa and 0.41 GPa at 2 K, indicating an electron-type conduction

in agreement with the ambient results.[19] With the increasing external pressure, the slope of the Hall resistance increases monotonically at 2 K and changes from negative to positive for 1.46 GPa, which implies a carrier-type inversion from electron- to hole-type. This could attribute to the change of the Fermi surface and viewed as a signature of the Lifshitz transition. In addition, the saturation value of ρ_{yx} at 300 K decreases slowly from 2.99 μΩ·cm at 0.69 GPa to 2.35 μΩ·cm at 7.11 GPa with the increasing pressure.

The Hall conductivity can be obtained from $\sigma_{xy} = \rho_{yx}/(\rho_{yx}^2 + \rho_{xx}^2)$.[19,24,44] Figures 4(a) and 4(b) display the corresponding AHC σ_{xy}^{A} at 200 K under different pressures in runs 1 and 2, respectively. In run 1, the saturation value of σ_{xy}^{A} is 326 $\Omega^{-1}\cdot\mathrm{cm}^{-1}$ at 0.69 GPa, comparable with 380 $\Omega^{-1}\cdot\mathrm{cm}^{-1}$ at ambient pressure.[19] However, with increasing pressure, the saturation value rapidly drops to about 65 $\Omega^{-1}\cdot\mathrm{cm}^{-1}$, and then remains almost unchanged. In run 2, the saturation value of σ_{xy}^{A} first increases and then slowly decreases. This may be related to the incomplete contact between electrical leads and the sample at 0.41 GPa due to the use of solid NaCl as pressure transmitting medium. It is generally accepted that the total AHC consists of three terms in ferromagnetic conductor: $\sigma_H^{\mathrm{A}} = \sigma_{\mathrm{int}} + \sigma_{\mathrm{sk}} + \sigma_{\mathrm{sj}}$, where σ_{int} is the intrinsic Karplus–Luttinger term, σ_{sk} is the extrinsic skew scattering, and σ_{sj} the generalized extrinsic side jump.[3,4] To separate the intrinsic from extrinsic contributions, we employ the so-called Tian–Ye–Jin (TYJ) scaling:[4,13] $\sigma_{xy}^{\mathrm{A}} = f(\sigma_{xx,0})\,\sigma_{xx}^2 + \sigma_{xy}^{\mathrm{int}}$, where $f(\sigma_{xx,0})$ is a function of the residual conductivity $\sigma_{xx,0}$, σ_{xx} is the longitudinal conductivity, and $\sigma_{xy}^{\mathrm{int}}$ is the intrinsic AHC. We plot the σ_{xy}^{A} as a function of σ_{xx}^2 for different pressures in Fig. 4(c). Because $\sigma_{xy}^{\mathrm{int}}$ does not depend on the scattering rate, $\sigma_{xy}^{\mathrm{int}}$ is then the remnant σ_{xy}^{A} that is observed as $\sigma_{xx}^2 \to 0$. The $\sigma_{xy}^{\mathrm{int}}$ as a function of pressure is displayed in Fig. 4(d). In run 1, the $\sigma_{xy}^{\mathrm{int}}$ decreases rapidly from 330 $\Omega^{-1}\cdot\mathrm{cm}^{-1}$ at 0.69 GPa to ∼65 $\Omega^{-1}\cdot\mathrm{cm}^{-1}$. With further compression, the $\sigma_{xy}^{\mathrm{int}}$ keeps at ∼65 $\Omega^{-1}\cdot\mathrm{cm}^{-1}$. In run 2, the $\sigma_{xy}^{\mathrm{int}}$ basically keeps at ∼150 $\Omega^{-1}\cdot\mathrm{cm}^{-1}$. As can be seen, the intrinsic AHC $\sigma_{xy}^{\mathrm{int}}$ of $LiMn_6Sn_6$ is robust at high pressure.

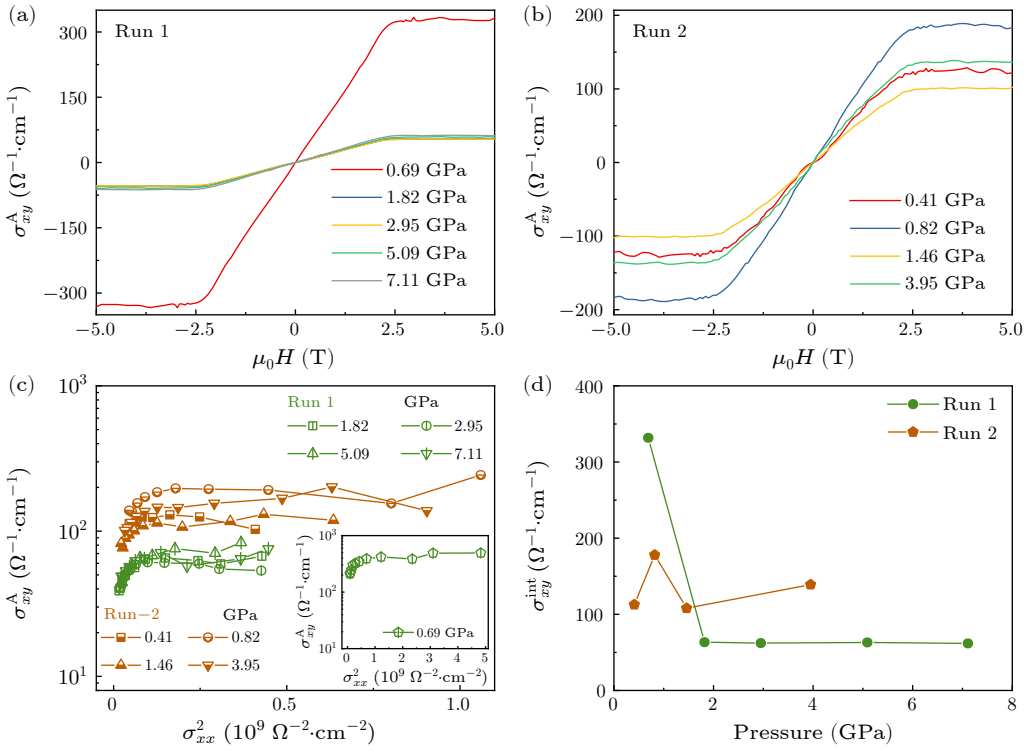

Fig. 4. Field-dependent anomalous Hall conductivity (AHC) σ_{xy}^{A} at 200 K for selected pressures in run 1 (a) and run 2 (b). (c) Plot of AHC σ_{xy}^{A} as a function of σ_{xx}^2. (d) Pressure-dependent intrinsic AHC $\sigma_{xy}^{\mathrm{int}}$ in the two runs.

To further understand the pressure effects, we performed the theoretical calculations. As the volume shrinks with pressure, there is almost no change for the electronic structure near the Fermi level, see the evolution of energy dispersion in Figs. 5(a)–5(d). Correspondingly, the distribution of the Ω_{yx} component of Berry curvature is also robust, see Figs. 5(e)–5(h). From the Berry curvature distribution, one can see that the three peaks of Ω_{yx} locate near K points and between A and L, which mainly originate from anti-crossings with tiny effective masses around the Fermi level. Since all the three peaks are positive, the integral of Berry curvature in the whole k-space gives a positive AHC around 180 $\Omega^{-1}\cdot\mathrm{cm}^{-1}$ at zero pressure, in good agreement with that from Hall measurement. In addition, the calculated magnetic moment of $LiMn_6Sn_6$ is around 2.54 μ_{B}/Mn, also close to the saturated magnetic moment (2.4 μ_{B}/Mn) at ambient pressure.[19] Consistent with the results of volume-dependent electronic band

structure and Berry curvature distributions, both magnetization and AHC are robust against pressure. As presented in Figs. 5(i) and 5(j)), the magnetic moment and AHC are limited in the ranges from $\sim 2.50\,\mu_B$/Mn to $\sim 2.54\,\mu_B$/Mn and from $\sim 180\,\Omega^{-1}\cdot\text{cm}^{-1}$ to $250\,\Omega^{-1}\cdot\text{cm}^{-1}$, respectively. Therefore, the stable AHE under perturbation of pressure in $LiMn_6Sn_6$ originates from the robust electronic and magnetic structure.

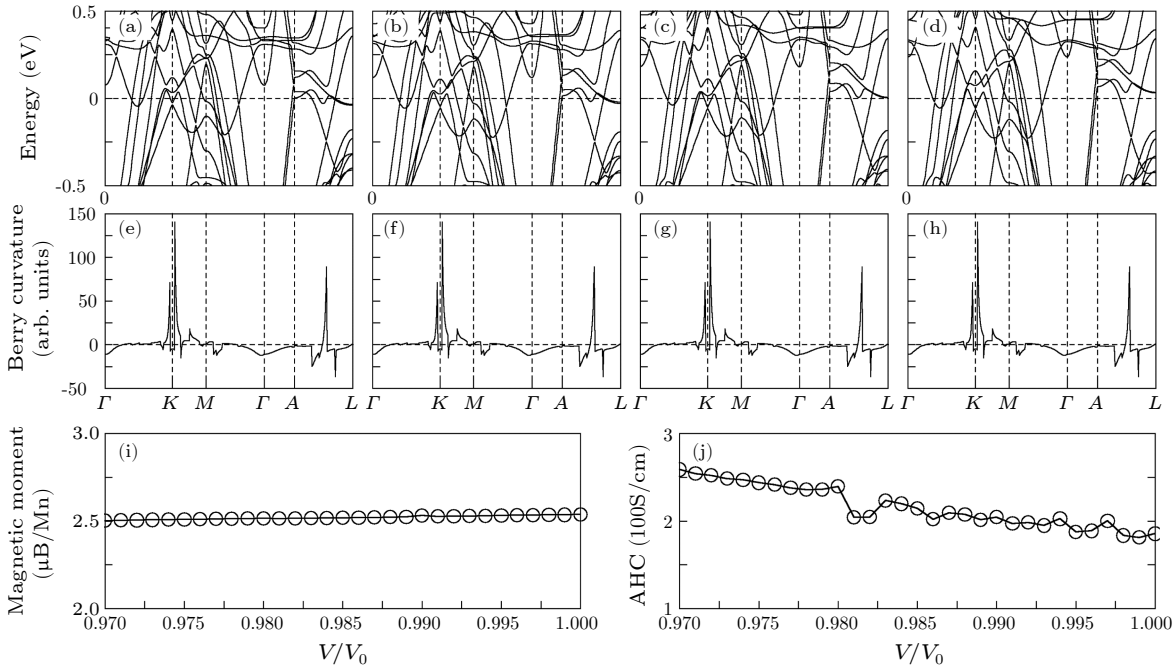

Fig. 5. Evolution of electronic structure, Berry curvature, magnetization, and AHC. (a)–(d) Energy dispersion along high symmetry lines for the cases of $V/V_0 = 1.00$, 0.99, 0.98, and 0.97, respectively. V_0 is the volume from experimental measurement at zero pressure. (e)–(h) Berry curvature (Ω_{yx} component) along high symmetry lines in the same condition with (a)–(d). [(i), (j)] Volume-dependent magnetic moment and anomalous AHC, respectively.

In conclusion, we have investigated the pressure effect on the AHE of $LiMn_6Sn_6$ by employing *in situ* high-pressure Raman spectroscopy, Hall transport measurements and first-principles calculations. The crystal structure and AHE of $LiMn_6Sn_6$ are robust under high pressure. According to the first-principles calculations, the stable AHE in $LiMn_6Sn_6$ originates from the robust electronic and magnetic structures under high pressure. This result shows that the AHC of $LiMn_6Sn_6$ is very stable under high pressure, which lays a good foundation for development of spintronic devices in extreme environment.

See the Supplementary Material for detailed data of physical properties of $LiMn_6Sn_6$ single crystals, magnetoresistance and Hall resistivity as a function of magnetic field at different pressures and temperatures in run 2.

Acknowledgments. This work was supported by the National Natural Science Foundation of China (Grant No. 52272265), the National Key R&D Program of China (Grant Nos. 2023YFA1607400 and 2018YFA0704300). Y.S. thanks the support from the National Natural Science Foundation of China (Grant Nos. 52271016 and 52188101). The authors thank the support from Analytical Instrumentation Center (# SPST-AIC10112914), SPST, ShanghaiTech University. C.F. thanks the European Research Council (ERC Advanced Grant No. 742068 'TOPMAT'), the DFG through SFB 1143 (Project ID 247310070), and the Würzburg-Dresden Cluster of Excellence on Complexity and Topology in Quantum Matter ct.qmat (EXC2147, Project ID 390858490).

References

[1] Hall E H 1880 *The London, Edinburgh, and Dublin Philosophical Magazine and Journal of Science* **10** 301
[2] Hall E H 1881 *The London, Edinburgh, and Dublin Philosophical Magazine and Journal of Science* **12** 157
[3] Nagaosa N, Sinova J, Onoda S, MacDonald A H, and Ong N P 2010 *Rev. Mod. Phys.* **82** 1539
[4] Tian Y, Ye L, and Jin X 2009 *Phys. Rev. Lett.* **103** 087206
[5] Berger L 1970 *Phys. Rev. B* **2** 4559
[6] Smit J 1955 *Physica* **21** 877
[7] Smit J 1958 *Physica* **24** 39
[8] Karplus R and Luttinger J M 1954 *Phys. Rev.* **95** 1154
[9] Kumar N, Guin S N, Manna K, Shekhar C, and Felser C 2021 *Chem. Rev.* **121** 2780
[10] Bernevig B A, Felser C, and Beidenkopf H 2022 *Nature* **603** 41
[11] Yin J X, Lian B, and Hasan M Z 2022 *Nature* **612** 647
[12] Wang Q, Sun S, Zhang X, Pang F, and Lei H 2016 *Phys. Rev. B* **94** 075135
[13] Ye L, Kang M, Liu J, von Cube F, Wicker C R, Suzuki T, Jozwiak C, Bostwick A, Rotenberg E, Bell D C, Fu L, Comin R, and Checkelsky J G 2018 *Nature* **555** 638
[14] Nakatsuji S, Kiyohara N, and Higo T 2015 *Nature* **527** 212
[15] Liu D F, Liang A J, Liu E K, Xu Q N, Li Y W, Chen C, Pei D, Shi W J, Mo S K, Dudin P, Kim T, Cacho C, Li G, Sun Y, Yang L X, Liu Z K, Parkin S S P, Felser C, and Chen Y L 2019 *Science* **365** 1282

[16] Liu E, Sun Y, Kumar N, Muechler L, Sun A, Jiao L, Yang S Y, Liu D, Liang A, Xu Q, Kroder J, Süß V, Borrmann H, Shekhar C, Wang Z, Xi C, Wang W, Schnelle W, Wirth S, Chen Y, Goennenwein S T B, and Felser C 2018 *Nat. Phys.* **14** 1125

[17] Wang Q, Xu Y, Lou R, Liu Z, Li M, Huang Y, Shen D, Weng H, Wang S, and Lei H 2018 *Nat. Commun.* **9** 3681

[18] Asaba T, Thomas S M, Curtis M, Thompson J D, Bauer E D, and Ronning F 2020 *Phys. Rev. B* **101** 174415

[19] Chen D, Le C, Fu C, Lin H, Schnelle W, Sun Y, and Felser C 2021 *Phys. Rev. B* **103** 144410

[20] Gu X, Chen C, Wei W S, Gao L L, Liu J Y, Du X, Pei D, Zhou J S, Xu R Z, Yin Z X, Zhao W X, Li Y D, Jozwiak C, Bostwick A, Rotenberg E, Backes D, Veiga L S I, Dhesi S, Hesjedal T, van der Laan G, Du H F, Jiang W J, Qi Y P, Li G, Shi W J, Liu Z K, Chen Y L, and Yang L X 2022 *Phys. Rev. B* **105** 155108

[21] Ma W, Xu X, Yin J X, Yang H, Zhou H, Cheng Z J, Huang Y, Qu Z, Wang F, Hasan M Z, and Jia S 2021 *Phys. Rev. Lett.* **126** 246602

[22] Yin J X, Ma W, Cochran T A, Xu X, Zhang S S, Tien H J, Shumiya N, Cheng G, Jiang K, Lian B, Song Z, Chang G, Belopolski I, Multer D, Litskevich M, Cheng Z J, Yang X P, Swidler B, Zhou H, Lin H, Neupert T, Wang Z, Yao N, Chang T R, Jia S, and Zahid Hasan M 2020 *Nature* **583** 533

[23] Wang Q, Neubauer K J, Duan C, Yin Q, Fujitsu S, Hosono H, Ye F, Zhang R, Chi S, Krycka K, Lei H, and Dai P 2021 *Phys. Rev. B* **103** 014416

[24] Gao L, Shen S, Wang Q, Shi W, Zhao Y, Li C, Cao W, Pei C, Ge J Y, Li G, Li J, Chen Y, Yan S, and Qi Y 2021 *Appl. Phys. Lett.* **119** 092405

[25] Mazet T, Ihou-Mouko H, Marêché J F, and Malaman B 2006 *Eur. Phys. J. B* **51** 173

[26] Mazet T, Venturini G, Welter R, and Malaman B 1998 *J. Alloys Compd.* **264** 71

[27] Wang Q, Kong P, Shi W, Pei C, Wen C, Gao L, Zhao Y, Yin Q, Wu Y, Li G, Lei H, Li J, Chen Y, Yan S, and Qi Y 2021 *Adv. Mater.* **33** 2102813

[28] Pei C, Ying T, Zhao Y, Gao L, Cao W, Li C, Hosono H, and Qi Y 2022 *Matter Radiat. Extremes* **7** 038404

[29] Pei C, Zhang J, Wang Q, Zhao Y, Gao L, Gong C, Tian S, Luo R, Li M, Yang W, Lu Z Y, Lei H, Liu K, and Qi Y 2023 *Natl. Sci. Rev.* **10** nwad034

[30] Pei C, Ying T, Zhang Q, Wu X, Yu T, Zhao Y, Gao L, Li C, Cao W, Zhang Q, Schnyder A P, Gu L, Chen X, Hosono H, and Qi Y 2022 *J. Am. Chem. Soc.* **144** 6208

[31] Chen X, Wang M, Gu C, Wang S, Zhou Y, An C, Zhou Y, Zhang B, Chen C, Yuan Y, Qi M, Zhang L, Zhou H, Zhou J, Yao Y, and Yang Z 2019 *Phys. Rev. B* **100** 165145

[32] Lee M, Kang W, Onose Y, Tokura Y, and Ong N P 2009 *Phys. Rev. Lett.* **102** 186601

[33] Liu Z Y, Zhang T, Xu S X, Yang P T, Wang Q, Lei H C, Sui Y, Uwatoko Y, Wang B S, Weng H M, Sun J P, and Cheng J G 2020 *Phys. Rev. Mater.* **4** 044203

[34] O'Hara D J, Brubaker Z E, Stillwell R L, O'Bannon E F, Baker A A, Weber D, Aji L B B, Goldberger J E, Kawakami R K, Zieve R J, Jeffries J R, and McCall S K 2020 *Phys. Rev. B* **102** 054405

[35] Wang X, Li Z, Zhang M, Hou T, Zhao J, Li L, Rahman A, Xu Z, Gong J, Chi Z, Dai R, Wang Z, Qiao Z, and Zhang Z 2019 *Phys. Rev. B* **100** 014407

[36] Zhou Y, Chen X, Zhou Y, Yu J, Zhu X, An C, Park C, Wan X, Yang X, and Yang Z 2022 *Sci. China Phys. Mech. Astron.* **65** 288211

[37] Gao L, Wu J, Xi M, Pei C, Wang Q, Zhao Y, Tian S, Li C, Cao W, Chen Y, Lei H, and Qi Y 2023 *Appl. Phys. Lett.* **122** 172404

[38] Mao H K, Xu J, and Bell P M 1986 *J. Geophys. Res.-Solid Earth* **91** 4673

[39] Kresse G and Furthmüller J 1996 *Phys. Rev. B* **54** 11169

[40] Perdew J P, Burke K, and Ernzerhof M 1996 *Phys. Rev. Lett.* **77** 3865

[41] Mostofi A A, Yates J R, Pizzi G, Lee Y S, Souza I, Vanderbilt D, and Marzari N 2014 *Comput. Phys. Commun.* **185** 2309

[42] Xiao D, Chang M C, and Niu Q 2010 *Rev. Mod. Phys.* **82** 1959

[43] Pei C, Jin S, Huang P, Vymazalova A, Gao L, Zhao Y, Cao W, Li C, Nemes-Incze P, Chen Y, Liu H, Li G, and Qi Y 2021 *npj Quantum Mater.* **6** 98

[44] Kong X, Tao Z, Zhang R, Xia W, Chen X, Pei C, Ying T, Qi Y, Guo Y, Yang X, and Li S 2024 *Chin. Phys. Lett.* **41** 047503